JOURNAL OF GUIDANCE, CONTROL, AND DYNAMICS
Vol. 25, No. 5, September–October 2002

Trajectory Optimization for Air-to-Surface Missiles with Imaging Radars

Asif Farooq*
MBDA UK, Ltd., Borehamwood, England WD6 1RX, United Kingdom
and
David J. N. Limebeer†
Imperial College, London, England SW7 2BT, United Kingdom

The use of trajectory optimization techniques is presented for the terminal guidance of an air-to-surface missile using a Doppler beam sharpening (DBS) radar seeker. The terminal guidance problem is characterized by a stealthy terrain-following phase that is followed by a climb and dive onto the target (a "bunt" trajectory). The imaging properties of DBS radars impose additional azimuth plane constraints on the trajectory that have to be incorporated into the optimization process. The various mission phases are interrelated, and the performance objectives come into conflict with the hardware constraints. The trajectory optimizer is used to generate offline open-loop controls that satisfy the various mission requirements. Numerical examples are used to illustrate the method and its efficacy.

Nomenclature

A_{mx}, A_{my}, A_{mz}	=	body axis accelerations achieved, ms^{-2}
A_{myd}, A_{mzd}	=	yaw and pitch acceleration demands, respectively, ms^{-2}
a	=	tuning parameter for imaging state constraint
a_0, a_1, a_2	=	coefficients for air density polynomial
C_{d0}	=	zero incidence drag coefficient
f_D, f_{DA}, f_{DB}	=	Doppler shifts, Hz
$f(t)$	=	function for Doppler beam sharpening imaging constraint
g	=	acceleration due to gravity, ms^{-2}
$\boldsymbol{i}, \boldsymbol{j}, \boldsymbol{k}$	=	space orientated unit vectors
J	=	performance index
m	=	mass of missile, kg
N	=	number of discretization intervals
p, q, r	=	roll, pitch, and yaw rates, $degs^{-1}$
R	=	range to go, m
$\boldsymbol{R}$	=	unit vector along sightline axis
R_b	=	bunt range, m
R_{exp}	=	downrange coordinate at which missile crosses exposure height, m
R_{sx}, R_{sy}, R_{sz}	=	downrange, crossrange, and altitude, respectively, m
$R_{sx}(T)$, $R_{sy}(T)$, $R_{sz}(T)$	=	final position calculated by optimizer, m
$R_{sx}(t_f)$, $R_{sy}(t_f)$, $R_{sz}(t_f)$	=	target coordinates, m
S	=	reference area, m^2
T	=	final time calculated by optimizer, s
T_i	=	incidence lag, s
T_{max}	=	maximum thrust, N
t_b	=	time at which missile becomes exposed, s
t_{exp}, t, t_f	=	exposure time, current time, and final time, respectively, s
V	=	total speed, ms^{-1}
V_{sx}, V_{sy}, V_{sz}	=	space frame components of the velocity vector, ms^{-1}
$\boldsymbol{v}$	=	velocity vector
X_A, Y_A, Z_A	=	sightline frame
X_B, Y_B, Z_B	=	body frame
X_I, Y_I, Z_I	=	missile inertial frame
X_S, Y_S, Z_S	=	Earth-fixed frame
x, y, z	=	target offset in downrange, crossrange, and altitude, respectively, m
α, β	=	angles of incidence and sideslip, respectively, deg
Γ	=	impact angle, deg
γ, χ	=	flight-path and heading angle, respectively, deg
Δ	=	crossrange resolution, m
δf	=	Doppler difference, Hz
δt	=	seeker coherent integration period, s
θ, ψ	=	pitch and yaw angles, deg
Λ	=	angle between target sightline and velocity vector in elevation, deg
λ	=	wavelength, m
λ_y, λ_z	=	sightline angles in azimuth and elevation, respectively, deg
Ξ	=	angle between target sightline and velocity vector in azimuth, deg
ρ	=	air density, kg m^{-3}
Φ	=	scaling parameter used in cost function
Ψ, Θ	=	azimuth and elevation look angles, respectively, deg
Ω	=	total angle between velocity and sightline, deg
ω, ζ	=	bandwidth, rad s^{-1}, and damping ratio of autopilot

Received 31 May 2001; revision received 1 February 2002; accepted for publication 26 March 2002.

*Systems Engineer, Seeker Division, Hertfordshire (formerly, Alenia Marconi Systems Ltd., Dynamics Division).

†Professor and Head, Department of Electrical and Electronic Engineering.

I. Introduction

THIS paper considers the use of trajectory optimization techniques for the terminal guidance control of a five-degree-of-freedom (5-DOF) air-to-surface missile with a radar imaging seeker. The terminal guidance phase will typically involve the last minute of flight, at about 15-km range, and will require the accurate determination of the target location and information about the optimal approach route to the target. A seeker will be used in conjunction with global positioning system (GPS) updates to determine the target

location. The seeker uses a high-resolution radar image to identify targets at ranges of 10–15 km. High resolution in downrange can be achieved using a narrow transmitted pulse, or by pulse compression techniques, and Doppler beam sharpening (DBS) processing can be used to achieve high crossrange resolution. This technique requires an angular offset between the velocity vector and the sightline vector in azimuth and usually gives rise to large crossrange offsets that impose constraints on the trajectory optimization problem. In addition to the imaging requirements, the missile is required to fly at low altitudes to avoid exposure to air defense systems. The stealthy approach is followed by a climb and dive (bunt maneuver). This maneuver is used to image the ground area and to achieve a prespecified impact angle. Impact and incidence angle constraints are used to maximize the effectiveness of direction sensitive warheads. Optimization in the final phase of flight is of paramount importance because it is necessary to balance the requirements associated with evading air defenses, satisfying terminal constraints and respecting the missile dynamics. Conventional methods of guidance such as proportional navigation (PN) have limitations in shaping a trajectory in highly constrained scenarios of this nature.

A. Previous Research

A lot of work has been done on the trajectory optimization of airborne vehicles. Bunt trajectories that make use of linear optimal control for terminal guidance have been reported in Ref. 1, where analytic means are used to determine a state feedback control law. In Ref. 2, linear quadratic techniques are used to achieve a terminal angle constraint for reentry vehicles. Both of these papers deal with the control constraints indirectly via terms in the cost function. An estimate of the time-to-go is needed to compute the feedback gains. There are several advantages of control laws that are derived from linear models: 1) They are in a state feedback form, 2) they can be designed to be robust,[3] and 3) they are easy to implement. In Ref. 4, the minimum principle is used, along with geometric considerations, to obtain an analytic solution for an air-to-surface missile guidance problem with an impact angle requirement. A point mass missile model and a first-order lag autopilot with control constraints are used. The optimal switching instants are determined numerically.

Nonlinear optimal control algorithms in conjunction with point mass models are used in Refs. 5 and 6 to study air-to-air scenarios. In Ref. 5, a trajectory synthesis problem is studied for an air-to-air missile with poststall maneuvering. A receding horizon strategy is used to generate a feedback mechanism. In Ref. 6 open-loop solutions are generated for the range maximization of an air-to-air missile with a fixed final time. The companion paper[7] uses a neighboring optimal control scheme to provide a feedback layer for closed-loop guidance, and a PN law is used in the terminal phase of flight. Trajectory planning with terrain following for aircraft and helicopters is reported in Refs. 8 and 9. An inverse dynamics approach is employed in Ref. 8 to solve a flight-time minimization problem with endpoint and terrain clearance constraints. The resulting control law is then implemented using nonlinear predictive control.[10]

A more recent approach, which is driven by the continued increases in processor speeds, generates the guidance commands by repeatedly solving a real-time optimization problem. This approach, in conjunction with a point mass model, is also considered in Ref. 11 for aircraft range maximization. Singular perturbation techniques are used to reduce the computational burden. Other papers[12,13] adapt optimal control algorithms to meet real-time guidance requirements. In Ref. 12 collocation is proposed and tested on a number of aerospace examples. In Ref. 13, multiple shooting, direct shooting, and collocation for spacecraft closed-loop guidance are compared in terms of reliability and flight processor requirements. Following Ref. 13, a guidance algorithm based on shooting and nonlinear programming is presented in Ref. 14 for an advanced launch system. In Ref. 15 differential inclusions are used to solve an online minimum time to the climb aircraft problem using an adaptive node refinement strategy. The nodes are densely placed in the vicinity of the current point and sparsely distributed over the rest of the horizon; the rationale is that the optimal control sequence should be based on local behavior. Simulations were then carried out to compare the online solution with a more accurate offline solution.

Online approaches have the advantage of being autonomous and are less reliant on extensive preflight analysis. If the terminal boundary conditions are modified substantially, or disturbances cause large deviations from a nominal preflight trajectory, these methods become even more attractive. Linear approximations for trajectory tracking are not needed, and mission flexibility may be enhanced. This adaptive guidance capability may be particularly important in the context of missile control problems, where uncertainties in target position and aerodynamic data, as well as new mission data, call for the repeated regeneration of trajectory profiles.

B. Current Research

Trajectory optimization studies for a simple missile autopilot/airframe model are presented. Our terminal guidance problem is characterized by pathwise state constraints (representing in-flight constraints), terminal equality constraints, control bounds, and a free final time. Numerical means are used to determine open-loop optimal trajectories. These open-loop optimal trajectories are useful as a benchmark for design purposes and can potentially be used as part of a closed-loop implementation.

A 5-DOF model that is described in Sec. II will be used in conjunction with a quadratic autopilot/airframe representation for the pitch and yaw freedoms. The calculation of optimal trajectories for the terminal guidance problem is essentially a nonlinear constrained optimization problem for which a multitude of techniques can be used. These range from the conventional (gradient and shooting methods) to more recent optimization algorithms. Obvious difficulties arise from conflicts between some of the objectives and constraints in the optimal control problem formulation of the terminal guidance problem. The model is given as a set of dynamic equations, and an objective function is minimized subject to pathwise state constraints, control bounds, and terminal trajectory constraints.

An optimization toolbox based on the algorithms described in Refs. 16–19 is used. The toolbox consists of a FORTRAN implementation of a sequential quadratic programming algorithm, specifically tailored to solve optimal control problems with state constraints. The optimization algorithm is coupled to an adaptive step size integration scheme for differential-algebraic systems. Convergence analysis and comparisons with other optimization packages on some sample optimal control problems may be found in Ref. 19. In the current problem, the physical limits likely to be encountered, such as look angle, g-capability, and incidence constraints, are dealt with naturally by this optimal control method. They are essentially state and control constraints. The control inputs to the system are the pitch and yaw acceleration demands. When a discretization scheme and an appropriate parameterization of the controls are invoked, trajectories that satisfy both the bunt and imaging requirements can be generated. The trajectories calculated for each test case will satisfy the necessary conditions for optimality, but they may not correspond to a global minimum. It turns out that there are multiple minima, and guaranteeing a global minimum is complex, computationally demanding, and possibly unnecessary. The extent to which the objectives are balanced depends critically on the scaling factors used in the problem. A description of the way in which the terminal guidance requirements are formulated and the scaling factors used is given in Sec. III. Section IV presents the results for two test cases with varying impact angle requirements, and some conclusions are drawn in Sec. V.

C. Terminal Guidance Problem and Method of Solution

The central requirements of the terminal guidance problem are to minimize both the miss distance and the exposure time to air defense systems. For direction sensitive warheads, a requirement in the elevation plane is the ability to hit the target at a specified impact angle. (This is measured from a vertical reference.) The ideal case corresponds to a zero impact angle and is commonly referred to as a "vertical" impact. The impact angle requirement is scenario dependent and, in the case of soft targets, may be relaxed. In many cases, the impact angle requirement necessitates a bunt maneuver of some kind. During the climb phase of the bunt, it will be necessary to image the target to determine its exact location. These data will be used to make final adjustments to the trajectory.

The trajectory optimization problem has to incorporate several constraints including 1) the vehicle's lateral acceleration capability, 2) the radar imaging constraints, 3) the seeker look angle constraints, and 4) the ground clearance. These constraints specifically determine the height needed to obtain a prespecified impact angle and the range required to perform a bunt maneuver.

Radar imaging guidance introduces an interesting control constraint because it requires an azimuth squint angle to enhance the crossrange resolution of the radar image. These details are covered in the Appendix. Unlike the other constraints, the radar imaging constraints cannot be implemented directly as control or state constraints. The difficulties arise from the offset requirements associated with the radar coming into conflict with the terminal constraints. One cannot simultaneously maintain a crossrange offset throughout the flight because the missile must commence terminal homing at some range-to-go.

II. Model

The system equations were derived for a symmetric skid-to-turn missile, which is assumed to be roll controlled. The model assumes that controllers for both the pitch and the yaw autopilots have been implemented and that the closed-loop autopilot/airframe characteristics can be represented by quadratic responses. This is a reasonable approximation for the closed-loop missile dynamics if higher frequency effects such as actuator dynamics and nonminimum phase effects can be neglected as shown in Ref. 20. Euler angles are used in the body-to-space transform; this means that zero impact angles cannot be achieved due to singularities. However, small nonzero impact angles can be specified and achieved without difficulty. Additional assumptions are as follows:

1) The missile is roll stabilized so that the roll angle is small enough to be neglected.

2) The antenna and sightline frames are coincident, that is, the seeker is pointing at the target throughout the flight. It is assumed that the target coordinates are known in advance and that the seeker is stabilized against body motion coupling effects.

3) The sightline and antenna frame do not roll.

4) The target is stationary.

5) Modeling errors and exogenous disturbances are neglected.

6) The terrain is flat and level.

7) The engine thrust is constant.

8) A zero incidence drag term is used to calculate the drag force.

9) The target has been acquired and recognized before the terminal guidance phase.

On the basis of these assumptions, the system equations can be written in state-space form as

$$\dot{R}_{sx} = V_{sx} \tag{1}$$

$$\dot{R}_{sy} = V_{sy} \tag{2}$$

$$\dot{R}_{sz} = V_{sz} \tag{3}$$

$$\dot{V}_{sx} = \cos(\theta)\cos(\psi)(A_{mx}) - \sin(\psi)(A_{my}) - \sin(\theta)\cos(\psi)(A_{mz}) \tag{4}$$

$$\dot{V}_{sy} = \cos(\theta)\sin(\psi)(A_{mx}) + \cos(\psi)(A_{my}) - \sin(\theta)\sin(\psi)(A_{mz}) \tag{5}$$

$$\dot{V}_{sz} = \sin(\theta)(A_{mx}) + \cos(\theta)(A_{mz}) \tag{6}$$

$$\ddot{A}_{my} = -2\zeta\omega(\dot{A}_{my}) - \omega^2(A_{my}) + \omega^2(A_{myd}) \tag{7}$$

$$\ddot{A}_{mz} = -2\zeta\omega(\dot{A}_{mz}) - \omega^2(A_{mz}) + \omega^2(A_{mzd}) - \omega^2 g\cos(\theta) \tag{8}$$

Table 1 Missile initial conditions

Parameter	Value
$R_{sx}(0)$, m	0
$R_{sy}(0)$, m	0
$R_{sz}(0)$, m	30
$V_{sx}(0)$, ms^{-1}	306
$V_{sy}(0)$, ms^{-1}	0
$V_{sz}(0)$, ms^{-1}	0
$A_{my}(0)$, ms^{-2}	0
$A_{mz}(0)$, ms^{-2}	0
$\dot{A}_{my}(0)$, ms^{-3}	0
$\dot{A}_{mz}(0)$, ms^{-3}	0
$\theta(0)$, deg	0
$\psi(0)$, deg	0
$\gamma(0)$, deg	0
$\chi(0)$, deg	0

$$\dot{\theta} = \frac{A_{mz} + T_i(\dot{A}_{mz})}{V} \tag{9}$$

$$\dot{\psi} = \frac{A_{my} + T_i(\dot{A}_{my})}{V\cos(\theta)} \tag{10}$$

$$V = \sqrt{V_{sx}^2 + V_{sy}^2 + V_{sz}^2} \tag{11}$$

$$A_{mx} = \frac{T_{\max}}{m} - g\sin(\theta) - \frac{\rho V^2 S C_{\mathrm{d0}}}{2m} \tag{12}$$

$$\rho = a_0 + a_1 R_{sz} + a_2 R_{sz}^2 \tag{13}$$

$$\gamma = \sin^{-1}\left(\frac{V_{sz}}{V}\right) \tag{14}$$

$$\chi = \tan^{-1}\left(\frac{V_{sy}}{V_{sx}}\right) \tag{15}$$

The air density variation with altitude is modeled by a second-order polynomial and is based on the atmosphere model provided in Ref. 21. The missile drag is approximated by using a zero incidence drag term. The following parameters are deemed to be representative of a conventional closed-loop autopilot design at a nominal flight condition:

$$\omega = 10\ \mathrm{rad\,s}^{-1}, \qquad \zeta = 0.7, \qquad T_i = 0.5\ \mathrm{s} \tag{16}$$

$$m = 500\ \mathrm{kg}, \qquad T_{\max} = 2500\ \mathrm{N}$$

$$C_{\mathrm{d0}} = 0.3, \qquad S = 0.132\ \mathrm{m}^2 \tag{17}$$

$$a_0 = 1.224, \qquad a_1 = -1.142 \times 10^{-4}, \qquad a_2 = 3.312 \times 10^{-9} \tag{18}$$

$$|A_{myd}, A_{mzd}| \leq 80\ \mathrm{ms}^{-2} \tag{19}$$

The two controls are the normal acceleration demands, A_{myd} and A_{mzd}. The missile initial conditions are shown in Table 1. The initial conditions describe a missile with an initial height of 30 m above the ground and a longitudinal speed of 306 ms^{-1} (Mach 0.9 at sea level). The missile is assumed to be flying straight and level.

A number of performance measures will be used to quantify the optimal trajectories. When $R_{sx}(T)$, $R_{sy}(T)$, and $R_{sz}(T)$ are denoted as the terminal downrange and altitude calculated by the optimizer as opposed to $R_{sx}(t_f)$, $R_{sy}(t_f)$, and $R_{sz}(t_f)$, which is the desired terminal position, the total miss distance is

$$\text{total miss} = \sqrt{[R_{sx}(T) - R_{sx}(t_f)]^2 + [R_{sy}(T) - R_{sy}(t_f)]^2 + [R_{sz}(T) - R_{sz}(t_f)]^2} \tag{20}$$

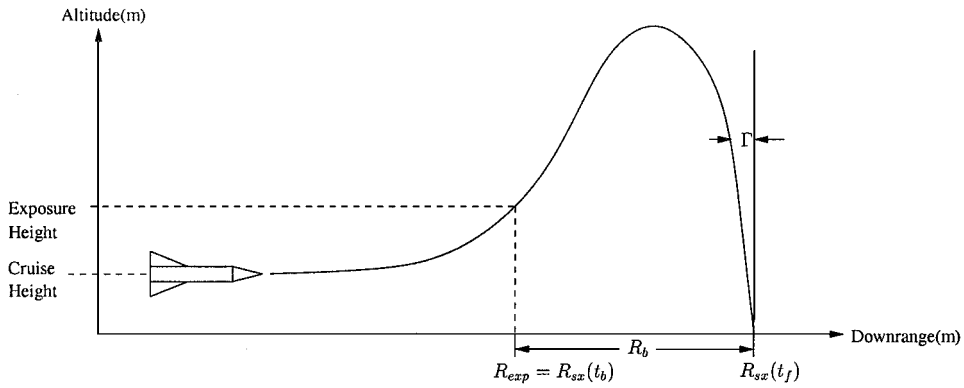

Fig. 1 Bunt maneuver definitions.

This is the miss distance computed when the integration algorithm stops and not the point of closest approach. The impact angle is defined as the trajectory slope at the final time and can be determined either from the space components of the velocity vector or the flight-path angle:

$$\Gamma = 90 - |\gamma(T)| \tag{21}$$

The exposure time is defined as the difference between the time the missile crosses a certain threshold height, for example, 100 m, denoted as t_b and the final time T calculated by the optimizer. The threshold height is assumed to be the height at which the missile becomes exposed to air defense systems and is otherwise arbitrary. This is shown in two dimensions in Fig. 1. The exposure time is, therefore,

$$t_{\text{exp}} = T - t_b \tag{22}$$

The bunt range is calculated as the difference between the terminal ground plane coordinates and the ground plane coordinates at which the missile crosses the exposure height threshold. When the latter is denoted by $R_{sx}(t_b)$ and $R_{sy}(t_b)$, the bunt range is

$$R_b = \sqrt{[R_{sx}(t_f) - R_{sx}(t_b)]^2 + [R_{sy}(t_f) - R_{sy}(t_b)]^2} \tag{23}$$

The distance-to-go coordinates are given by

$$x = R_{sx}(t) - R_{sx}(t_f) \tag{24}$$

$$y = R_{sy}(t) - R_{sy}(t_f) \tag{25}$$

$$z = R_{sz}(t_f) - R_{sz}(t) \tag{26}$$

The range to the target is, therefore,

$$R = \sqrt{x^2 + y^2 + z^2} \tag{27}$$

and the pitch and yaw sightline angles are defined as

$$\lambda_z = \sin^{-1}(z/R) \tag{28}$$

$$\lambda_y = \tan^{-1}(y/x) \tag{29}$$

The calculation of the seeker look angles can be shown to be

$$\Psi = c^{-1}[s(\lambda_y)s(\psi) + c(\lambda_y)c(\psi)] \tag{30}$$

$$\Theta = -c^{-1}[s(\lambda_z)c(\lambda_y)s(\theta)c(\psi) + s(\lambda_y)s(\lambda_z)s(\theta)s(\psi) + c(\lambda_z)c(\theta)] \tag{31}$$

where we denoted cos( ) by c( ), sin( ) by s( ), $\cos^{-1}$( ) by c^{-1}( ) and $\sin^{-1}$( ) by s^{-1}( ). Similarly, the angles between the sightline and velocity vector in azimuth and elevation can be shown to be

$$\Xi = c^{-1}[s(\lambda_y)s(\chi) + c(\lambda_y)c(\chi)] \tag{32}$$

$$\Lambda = -c^{-1}[s(\lambda_z)c(\lambda_y)s(\gamma)c(\chi) + s(\lambda_y)s(\lambda_z)s(\gamma)s(\chi) + c(\lambda_z)c(\gamma)] \tag{33}$$

The time for the terminal guidance run is defined as the time-to-go when the range to the target is less than 2 km. This is the time/range at which the radar imaging data would facilitate a reversion to another guidance method because it is not possible to image and home in on the target at very short ranges.

III. Optimal Control Formulation

Attention is now turned to the way in which the DBS and bunt requirements are formulated as an optimal control problem. The detailed choice of the cost function and the problem scaling factors have a major influence on the solution. To achieve adequate crossrange resolution from DBS radar imaging, a minimum value of angle in azimuth has to be maintained between the missile velocity vector and the sightline vector from the missile to the target. Some means of translating this into a form suitable for optimization is required. The generation of optimal trajectories can be envisaged as a multi-objective optimization problem in which some of the objectives, for example, miss distance, take precedence over others. The problem needs to be carefully formulated and scaled to ensure that the optimal controls take account of all of the (conflicting) problem requirements, some of which are 1) the minimization of the miss distance, 2) the minimization of the exposure time, 3) the minimization of the maximum height, 4) the minimization of the impact angle, 5) the maintenance of a sufficient angular offset for radar imaging purposes, 6) keeping the target in view throughout the bunt maneuver (seeker look angle constraint), 7) the maintenance of adequate ground clearance during terrain following, 8) ensuring that none of the missile's physical limits are exceeded during the bunt maneuver, and 9) smooth controls for both autopilots that are easy to implement.

Many of the tradeoffs are scenario dependent. For instance, the requirement of steep impact angles may be less important for soft targets in which case the exposure time could be reduced. In the case of systems using GPS, it is possible that the elevation look angle constraint can be relaxed because it may be possible for the target to move out of view for a fraction of the flight. These tradeoffs are essentially balanced by the scaling factors introduced in the optimal control formulation. It is generally difficult to determine whether a set of terminal conditions is feasible, given the physical constraints, for example, g-capability and look angle limits. The approach taken here is to specify a relaxed set of requirements and use this as a basis for approaching more stringent performance specifications. When issues of robustness are considered, it may well be preferable to sacrifice some performance by using a relaxed formulation. The crossrange resolution obtained using DBS processing (Appendix) can be shown to be

$$\Delta = \frac{R\lambda}{2V(\delta t)\sin(\Xi)\cos(\Lambda)} \tag{34}$$

Note that the crossrange resolution is inversely proportional to the azimuth squint angle Ξ. For optimization purposes the following approximation was used for the crossrange resolution:

$$\Delta \approx \frac{\lambda(x^2 + y^2)}{2V(\delta t)y} \tag{35}$$

because it is better behaved numerically than the true expression (34). The difficulty with Eq. (34) stems from that Ξ and Λ are complicated functions of the body attitude and the sightline angles, and this can result in numerical difficulties when Ξ is small or Λ is near 90 deg. With the crossrange resolution and model equations specified, the optimal control problem is now formulated. To control the missile height and crossrange position, the following performance index was investigated:

$$J = \int_0^T \left[(R_{sz} - 20)^2 + \Phi(R_{sy})^2\right] \mathrm{d}t \tag{36}$$

The first term effectively penalizes altitude deviations from a reference datum of 20 m; the weighting factor Φ is constant. The second term penalizes substantial deviations in crossrange and is used to "encourage" a large crossrange offset. In summary, minimizing the cost function reduces exposure to air defense units (ADUs), through the first term, whereas the second term maintains a high DBS crossrange resolution. In reality, this is somewhat simplistic because detection would be dependent on other factors such as the aspect angle, range to an ADU, and the radar cross section of the missile. We will disregard these issues here. The following terminal equality constraints are also prescribed:

$$R_{sx}(t_f) = 15{,}000 \tag{37}$$

$$R_{sy}(t_f) = 5000 \tag{38}$$

$$R_{sz}(t_f) = 20 \tag{39}$$

$$\gamma(t_f) = -69 \tag{40}$$

$$\theta(t_f) = -69 \tag{41}$$

These constraints specify the terminal position coordinates and the elevation angles at impact. These values are based on estimates of the terminal guidance phase of a typical mission, which would start at 15–20 km from the target. It is more difficult to estimate the crossrange offset: we choose a 5-km offset for this problem because this value, from the initial geometry, does not transgress any azimuth look angle constraints. It also results in an initial crossrange resolution of less than 2.5 m, for realistic values (0.3–0.5 s) of the seeker coherent integration period δt, which should be sufficient for target acquisition and recognition (assumption 9 in Sec. II). Other crossrange offsets can be imposed without difficulty. In the most extreme case, there would be no offset, and the missile may have to move away from the target in the azimuth plane, while not violating any seeker look angle constraints. This would enable the seeker to form a high-resolution image of the terrain, before homing in, but is potentially a more difficult problem because the initial crossrange resolution may be poor. Because the flight path and body attitude at impact are required to be the same value effectively minimizes any incidence at impact. All of those mentioned are hard constraints and require accurate controls. State constraints on the seeker azimuth and elevation look angles are also specified. The antenna is typically gimballed so these constraints are necessary to prevent the antenna servo from operating at its limit and to keep the target within the seeker field of view:

$$\Theta(t) \geq -40, \qquad \forall\, t \in [0, T] \tag{42}$$

$$\Psi(t) \leq 40, \qquad \forall\, t \in [0, T] \tag{43}$$

Note that the elevation look angle is negative as the missile is above the target. During the descent phase of the bunt maneuver, the elevation look angle steadily decreases to zero, as the sightline and body axes become aligned. Similarly, from the initial geometry, the azimuth look angle is positive and should remain positive, with a gradual reduction to zero near the impact point. Simulations confirmed that, at this stage, these constraints need only to be imposed in one direction. A ground clearance constraint is required that prevents a collision between the missile and the ground terrain. We used

$$R_{sz}(t) \geq 10, \qquad \forall\, t \in [0, T] \tag{44}$$

Because the target aim offpoint is 20 m above the ground, the state constraint (44) is not in conflict with the terminal z position requirement (39). The case where the target is at ground level can also be accommodated, but it requires a slightly more complicated function for the state constraint, for example, a function that is offset by 10 m and decreases rapidly near the terminal downrange. There may be advantages in selecting an aim-off point above the target and switching to a closed-loop guidance law during the final few seconds of flight.

The DBS imaging requirements are for high-resolution imaging up to the terminal guidance run. This facilitates the accurate selection of an aim point on the target at the point of handover. Note that large crossrange offsets do not always provide good crossrange resolution. This follows from that the missile's velocity and the sightline vectors can be closely aligned even if there is a large crossrange offset. With this in mind, the DBS constraints were enforced via an additional state constraint that makes use of the approximate crossrange resolution expression. We choose a suitable function, in this case an exponential, which specifies the minimum crossrange resolution as a continuous function of the crossrange co-ordinate. The DBS constraints are then handled by this one additional state constraint. Our choice of function is as follows:

$$f(t) = 0.1 + 2.6\exp(-R_{sy}/a), \qquad a = 800 \tag{45}$$

The value of the parameter a controls the tradeoff between high-resolution imaging and the bunt characteristic: A low value of a emphasizes imaging. In contrast, a high value of a will put less emphasis on imaging, and the trajectory in the azimuth plane will be similar to that associated with PN. The imaging constraint is, therefore,

$$\Delta - f(t) \leq 0.0, \qquad \forall\, t \in [0, T] \tag{46}$$

A. Choice of Initial Controls and Final Time

The optimal control problem can be recast as a nonlinear programming problem by parameterizing the controls and discretizing time. To facilitate rapid convergence, we also require sensible estimates for the final time and the initial controls. The choice of the first control (for the pitch autopilot) is straightforward and is chosen as the control that results in straight and level flight. Because gravity is included, we have

$$A_{mzd}(t) = 9.81, \qquad \forall\, t \in [0, T] \tag{47}$$

The second control (for the yaw autopilot) and the final time are dependent on the range to the target. Based on the initial geometry and initial missile speed, we can calculate the following underestimate for the final time:

$$T \geq \frac{\sqrt{15{,}000^2 + 5000^2}}{306} = 52 \tag{48}$$

because the bunt maneuver will increase the total flight time and full thrust is assumed. In fact, for the initial speed of 306 ms^{-1}, the thrust and drag tend to cancel one another so that a constant speed approximation is not an unreasonable one. We used this value as the initial estimate of the final time. Finally, it is necessary to provide an estimate for the initial yaw control, given that there is a large (5-km) crossrange offset. From elementary mechanics, the crossrange offset can be written

$$y = \tfrac{1}{2} A_{myd} T^2 \tag{49}$$

When the values for the final time and the crossrange offset are substituted, and rounded up,

$$A_{myd}(t) = 4.0, \qquad \forall\, t \in [0, T] \tag{50}$$

Table 2 Scaling factors

Constraint	Scaling factor
Terminal x position	1.0
Terminal y position	1.0
Terminal z position	1.0
Terminal body attitude	100.0
Terminal flight-path angle	100.0
Ground clearance state constraint	1.0
DBS imaging state constraint	100.0
Seeker look angle constraints	1000.0
Cost function	10^{-7}

The choice of initial controls and final time takes the missile close to the terminal position on the first iteration, but neither the imaging requirement nor the impact angle requirements are satisfied.

B. Scaling Factors

To balance the conflicting requirements in the constrained optimal control problem, it is usually necessary to introduce some scaling. The initial choice of controls, that is, $A_{myd} = 4$ ms^{-2} and $A_{mzd} = 9.81$ ms^{-2}, ensure that the constraint violations in each of the three terminal position variables will be of roughly equal order. The choice of initial controls will also cause the missile to hold its initial height. For these reasons, the weightings on the three terminal position constraints were chosen equal. By the same token, the ground clearance state constraint was given a unity weight. The remaining quantities, some of which are angles expressed in radians, require increased emphasis. The multipliers shown in Table 2 were found by trial and worked well in the examples.

C. Method of Solution

The common numerical techniques for solving an optimal control problem are the so-called direct and indirect techniques. Indirect techniques are known to be highly accurate but require substantial preanalysis and may be difficult to apply to complex problems. In this study, a direct method was used. Direct methods discretize time, the states, and the controls and use some functional approximation for the control variables, for example, piecewise constant functions or splines. In this way, the original problem can be recast as a nonlinear programming problem. Full discretization involves parameterizing both the states and controls by using a collocation scheme, and the associated state and control parameters are treated as unknowns in the nonlinear programming problem. An alternative method (sometimes called direct shooting), which results in a smaller sized problem, is to determine the states recursively using a higher-order integration scheme and to search in the control space for a solution. Both methods result in a finite dimensional nonlinear programming problem, although full discretization will result in a large sparse problem, necessitating the use of sparse matrix methods. Solutions can be obtained by applying a nonlinear programming algorithm such as sequential quadratic programming.

In this study, the direct shooting method was employed, and the controls are parameterized using piecewise constant functions. For example, the pitch control is represented as

$$A_{mzd}(t) = \sum_{i=1}^{N} p_i(t) A_{mzd_i}, \qquad \forall t \in [0, T], \quad i = 1, 2, \ldots, N \tag{51}$$

in which the A_{mzd_i} are constants and $p_i(t) = 1.0$, $t_i \le t \le t_{i+1}$, and 0 elsewhere. Each t_i is given by iT/N. A similar parameterization is applied for the yaw control. The states are determined using a Radau IIA integration algorithm for differential-algebraic systems. (See Ref. 19 for further details.) Gradients are determined by the backward integration of an adjoint system of equations. The values of A_{mzd_i} are then adjusted at each iteration using a sequential quadratic programming algorithm to minimize the cost function and satisfy the constraints. In this study, the computations were performed using double-precision arithmetic on a Sun SPARC workstation. Table 3 shows the values that were used for the convergence criteria, the integration tolerances, and the number of discretization intervals.

Table 3 Optimization parameters

Parameter	Value
Number of intervals for each control	400
Integration absolute tolerance	10^{-3}
Integration relative tolerance	10^{-3}
Convergence criteria	10^{-5}

This means that, for any solution, all of the constraints are satisfied with a tolerance of 10^{-5}. As explained in Ref. 19, approximation errors can be eliminated by reducing the integration tolerances and rerunning the optimization algorithm with the converged control as the initial guess. (This is similar to grid refinement techniques.) For the results in this study, this refinement step was not carried out because the solutions obtained were already thought to be sufficiently accurate for our purposes.

IV. Results

Results are given for two test cases with different impact angles. These studies will serve to reenforce the use of optimal control ideas in this type of work, as well as illustrate the sensitivity of the solution to the impact angle specification. In the same way, other performance parameters such as the bunt range and the maximum height can also be examined in conjunction with the DBS imaging requirements. We assume the following value for the K-band radar wavelength:

$$\lambda = 0.0085 \tag{52}$$

The following range of values are assumed for the seeker coherent integration period:

$$0.3 \le \delta t \le 0.5 \tag{53}$$

Three discrete values of integration period will be considered (0.3, 0.4, and 0.5 s), and the results compare the effect of varying this parameter. A larger value of δt corresponds to an increased synthetic diameter with a corresponding improvement in crossrange resolution. As explained in the Appendix, it is impossible to perform DBS imaging on the target throughout the engagement, and so a final guidance phase must be used to home in on the target when the crossrange resolution degrades. For these reasons, we assume that at a certain range from the target (approximately 2 km) the missile switches from DBS mode to a conventional guidance method because beyond this range there is an increased level of conflict between imaging and terminal guidance. A high-resolution image of the target near this range will be required. Our results will confirm that a range of 2 km is sufficient for adequate crossrange resolution, without compromising the terminal guidance requirements of small miss distances and terminal angle constraints.

In the first case, we specify a terminal impact angle of 21 deg. This is sufficient for some targets, and we will refer to it as the nominal case. The constraints and cost function are those described in Sec. III. Figure 2 shows the optimal trajectory in three dimensions, as well as its projection onto the ground plane. This shows that the missile follows a ground-hugging trajectory for over 10 km before the commencement of the bunt maneuver, which begins at approximately 10 km downrange and 1.7 km crossrange. The crossrange, altitude, and optimal controls are shown in Fig. 3. In each case, these quantities are expressed as functions of the downrange. The azimuth angle between the velocity and sightline as well as the crossrange resolution, for three values of DBS integration period, are shown in Fig. 4 as a function of the range-to-go.

In the second case, the impact angle is changed to examine the sensitivity of the solution to a more demanding specification in this terminal performance parameter. As explained in the Introduction, we would expect there to be some conflict between achieving a small impact angle, while performing high-resolution imaging. The following constraints are modified (as compared with case A):

$$\gamma(t_f) = -85 \tag{54}$$

$$\theta(t_f) = -85 \tag{55}$$

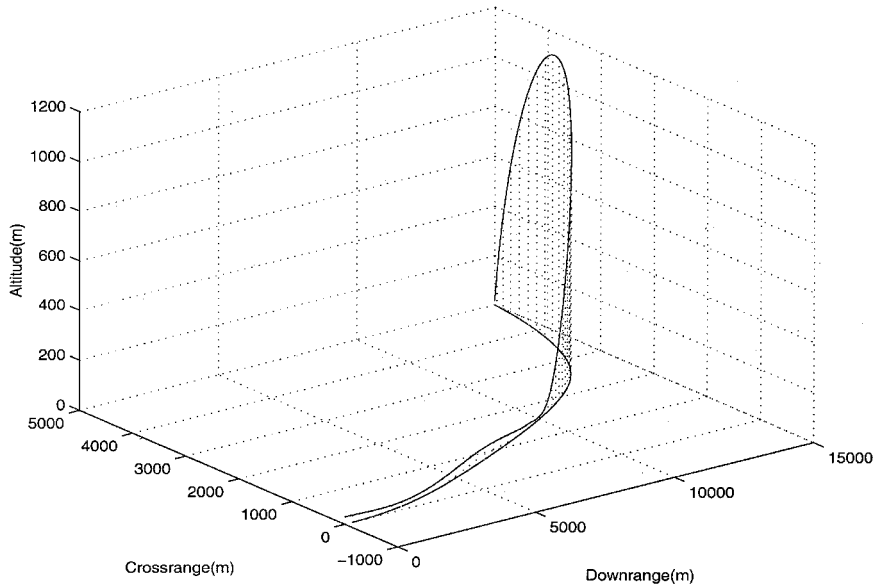

Fig. 2 Three-dimensional trajectory for case A.

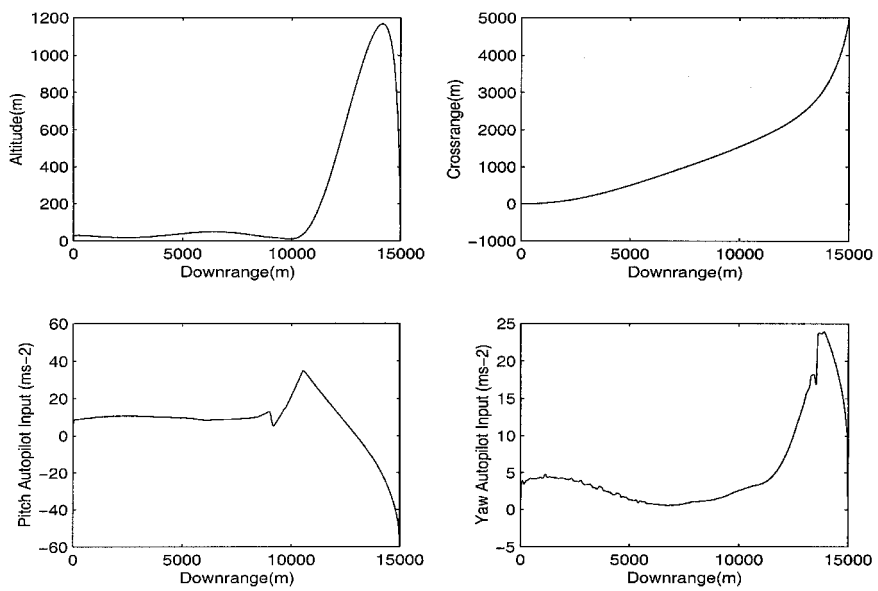

Fig. 3 States and controls for case A.

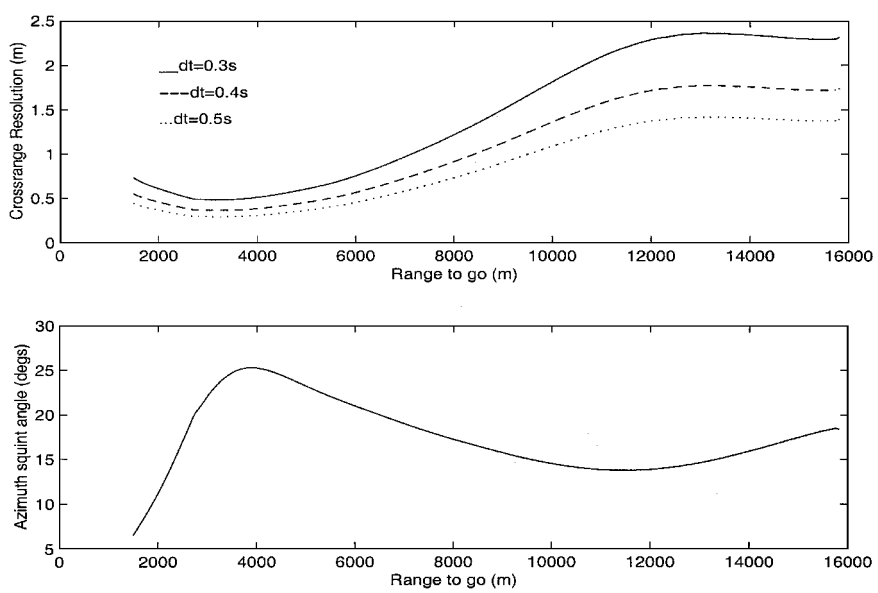

Fig. 4 Crossrange resolution and azimuth angle for case A.

The other constraints remain unchanged. It can be seen from the three-dimensional plot of the trajectory in Fig. 5 that the terrain-following phase occupies the first 10 km of downrange and that the bunt maneuver begins immediately thereafter. In this case, the peak height increases to just over 1300 m. The state trajectories and controls are shown in Fig. 6. The overall performance for the two test cases is shown in Table 4.

Table 4 shows that in both cases all of the terminal constraints are satisfied with no state constraint violations. Figures 3 and 6 show that the pitch control maintains its 9.81-ms^{-2} upward acceleration demand for straight and level flight until the bunt range is reached. At this point, following a brief dip, the pitch acceleration demand increases, thereby forcing the missile into a steep climb. There then follows a decrease in the normal acceleration demand to turn the missile over at the apogee and accelerate it onto the target. The maximum negative acceleration demand is required near the final time. The pitch control experiences a return to near zero demand at the final time to "wash out" any pitch plane incidence. In the azimuth plane very little yaw control is used in the first 10 km of downrange. There then follows a gradual increase to a maximum value of (23.94 ms^{-2} in case A compared with 24.53 ms^{-2} in case B). This is used to align the velocity and sightline vectors in azimuth to satisfy terminal position requirements. The controls are relatively smooth for both test cases. For case B, the 16-deg tightening in the impact angle requires around 160 m of extra height, an increase in flight time, and a slight increase in exposure time. The seeker elevation look angle is increased by around 6–39 deg, and the maximum acceleration demand for the pitch autopilot is increased by approximately 12.75 ms^{-2}. The increase in the bunt height reduces the impact speed by approximately 8 ms^{-1}. Although a lower speed

Table 4 Performance for both test cases

Performance measure	Case A	Case B
Miss distance, m	1.08×10^{-5}	4.59×10^{-6}
Time for terminal guidance run, s	7.39	7.89
Maximum height, m	1168	1327
Exposure time, s	21.0	21.89
Bunt range, m	5184	5073
Impact angle, deg	21.0	5.0
Incidence at impact, deg	0.0	0.0
Maximum azimuth look angle, deg	24.7	24.9
Maximum elevation look angle, deg	33.52	39.33
Maximum g (pitch)	3.56/−5.47	3.79/−6.77
Maximum g (yaw)	2.44/−0.03	2.50/−0.15
Impact speed, ms^{-1}	305	297
Final time, s	56.68	57.96

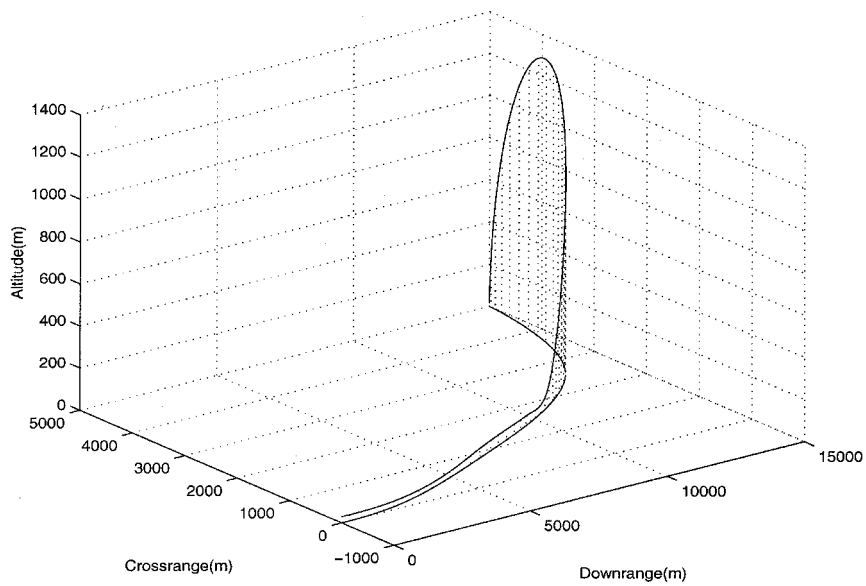

Fig. 5 Three-dimensional trajectory for case B.

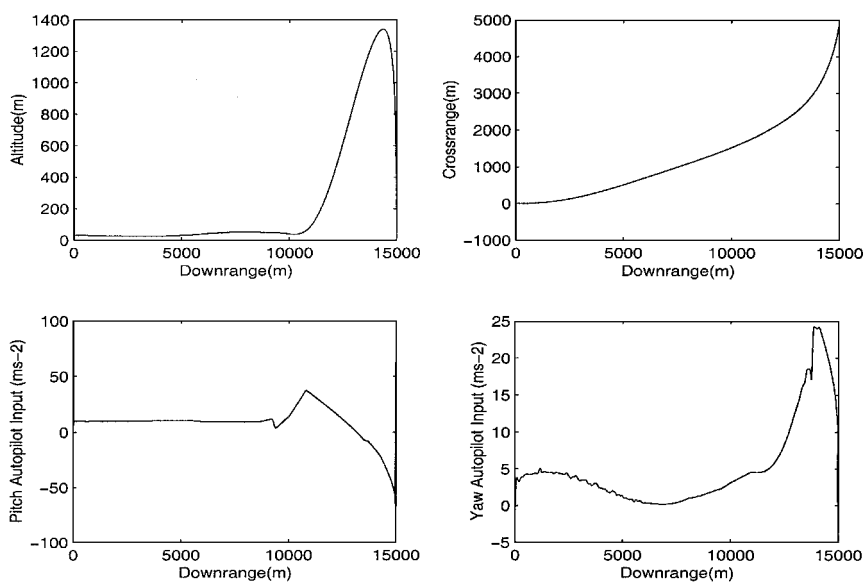

Fig. 6 States and controls for case B.

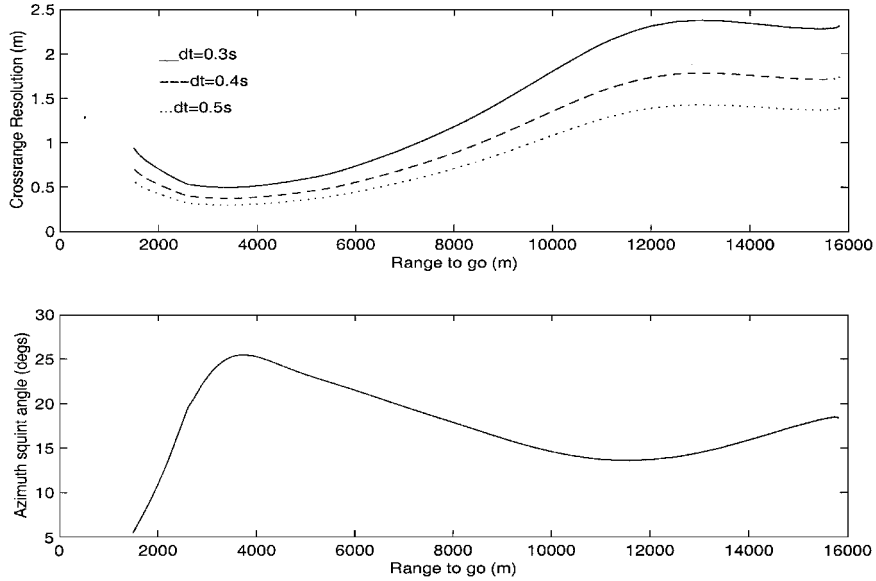

Fig. 7 Crossrange resolution and azimuth angle for case B.

Table 5 Crossrange resolution (meters) at 2 km for various DBS integration periods

Case	$\delta t = 0.3$ s	$\delta t = 0.4$ s	$\delta t = 0.5$ s
A	0.61	0.46	0.36
B	0.70	0.53	0.42

during the bunt increases vulnerability, this speed reduction can be used to increase the rate of turn [see Eq. (9)].

The azimuth angle between the velocity and sightline and the crossrange resolution (for various DBS integration periods) are plotted against range-to-go in Figs. 4 and 7. It can be seen from these diagrams that the angle between the sightline and velocity vector in azimuth has a maximum at approximately 4-km range-to-go for both test cases, before decreasing to approximately 10 deg at 2-km range-to-go. Each choice of integration period has a minima for the crossrange resolution at roughly 3-km range-to-go. As explained in the Appendix, this is a necessary consequence of the terminal constraints. To home in on the target, the velocity and sightline vectors must become aligned at some range-to-go. As the angular offset in azimuth reduces, the crossrange resolution will increase. The velocity vector and sightline vector in azimuth become aligned approximately 600 m from the target. This is not shown in any of the figures due to the singularity at this point. The crossrange resolution starts to increase rapidly at a range of around 1.5 km as this singularity is approached. The final time is increased by roughly 6.0 s from our initial guess, and further simulations show this increase is principally due to the DBS imaging requirement, rather than the bunt maneuver. In other words, the need to maintain a large crossrange offset increases the flight time. In terms of the imaging requirements at 2-km range, the crossrange resolution for both the test cases is stated in Table 5 for various values of the DBS integration period. For case A at 2-km range-to-go, the crossrange resolution is 0.61 m for the integration period of 0.3 s, improving to 0.36 m for an integration period of 0.5 s. For case B, there is a slight degradation in crossrange resolution as a function of range-to-go; this is due to the increase in the maximum height. The degradation is more marked for the smaller integration period of 0.3 s. Ideally, the crossrange resolution would be sufficient at 2 km for aim-point selection, although this is dependent on factors outside of trajectory control. The lower integration period of 0.3 s may require DBS imaging to a shorter range than 2 km in both test cases, which may run into conflict with the terminal guidance requirements. Similarly, for case B, the crossrange resolution for the integration period of 0.4 s may need to be improved. This could be done by tightening the radar imaging specifications further in the optimization process. Again, this is likely to impinge on the constraints in the elevation plane. We would expect the exposure time to be increased (inasmuch as an azimuth offset may need to be maintained for a longer period) and the bunt trajectory to be altered. Given that the maximum acceleration used is well within the limits imposed, further performance improvements may be possible. It is somewhat surprising that more control effort is not used in the azimuth plane where a large acceleration correction may be needed to home in on the target; this appears to be because the azimuth angle between the velocity and sightline is gradually reduced to zero to hit the target, with a resultant smooth control action.

In summary, the bunt maneuver with the tighter performance specification associated with case B is achievable without a significant degradation in exposure time. With that said, the physical constraints on the missile hardware are significantly increased with 1 g of extra pitching capability, as well as an increased seeker elevation look angle. When disturbances and modeling errors are considered, these hardware specifications may well escalate further. In terms of imaging, seeker coherent integration periods of 0.5 and 0.4 s would be acceptable for both cases because both of these integration periods are able to achieve acceptable crossrange resolution at a range of 2–3 km. For the lowest value of seeker integration period (0.3 s), further optimization may be required to achieve lower values of crossrange resolution, requiring a more aggressive trajectory in the azimuth plane.

V. Conclusions

The paper addresses the problem of calculating optimal controls for a missile with a radar imaging seeker using DBS. The problem requirements are translated into an optimal control problem that can then be solved using numerical optimization. Optimal controls were sought that balance the problem tradeoffs including low exposure times, steep impact angles, and high-resolution imaging. By applying a trajectory optimization method, we were able to calculate trajectories that allowed a high-resolution radar image to be formed, thereby enabling target detection, recognition, and aim-point selection. Various values of the seeker coherent integration period were examined to determine the sensitivity of the imaging capability to this parameter. Two test cases were examined with different impact angle requirements. When the two cases are compared, it can be seen that the optimal controls exhibit a predictable structure: the pitch control builds to a peak positive acceleration demand that is followed by the gradual use of a negative acceleration demand that turns the missile at the apogee. A return to zero control at the final time is necessary to minimize the incidence at impact. The yaw acceleration demand requires less control effort (under 3 g) by virtue of the problem geometry. With that said, it is conceivable that an increase in maximum lateral control effort could be used to improve further the crossrange resolution, thereby producing a sharper turn

in the azimuth plane. Seeker coherent integration periods of 0.4 and 0.5 s are acceptable in terms of achieving high crossrange resolution at ranges of 2–3 km for target aim-point selection. The results show that steeper impact angles compromise the crossrange resolution, as well as requiring an increase in the maximum height, the maximum elevation look angle, and the total flight time. Despite this, the solutions obtained achieve an acceptable compromise between the various performance specifications such as high-resolution imaging, low exposure times, and low impact angles without transgressing any realistic physical limits. In a practical situation it is advisable to leave some "slack" in the in-flight constraints and some additional control authority as noise and modeling errors must be accommodated.

Appendix: DBS Equations

DBS is a form of synthetic aperture radar that can be used to obtain high crossrange resolution. The equations needed to represent the DBS concept used for radar imaging are detailed in this section. A more detailed description of synthetic aperture radar and the associated radar signal processing may be found in Ref. 22 (Chapter 7), Ref. 23 (pp. 616–652), and Ref. 24. We derive the relevant DBS equations to use in the optimal control formulation using basic radar principles and the problem geometry. Difficulties inherent in DBS radars such as motion compensation, speckle, signal processing, and target detection and recognition are not considered in this paper. Some of these details can be appended at a later stage, but the main purpose is to consider the geometrical constraints DBS radars impose on the trajectory optimization problem and the way in which these constraints interact with the overall terminal guidance problem. This can be used as a benchmark for a more detailed analysis.

Consider the scenario shown in Fig. A1, where a missile using a radar imaging seeker is flying at a fixed height above the ground with the antenna beam illuminating an area on the ground. The downrange resolution is determined by the transmitter pulse width. Narrow pulses, or longer pulses that use pulse compression techniques, result in fine downrange resolutions. For high crossrange resolution, a large antenna diameter can be synthesized by storing and processing pulses over an appropriate length of the flight path. The processing requires amplitude and phase information to be stored from each scatterer to form a radar image of the ground area, which can be used to form a narrow synthetic beam. During the seeker coherent integration period, pulse returns within a range bin can be resolved into a number of Doppler frequencies (because they have different Doppler shifts). This enables a high-resolution image of the ground area to be formed. For terminal guidance purposes, finer resolution cells are required as the engagement proceeds for target detection, recognition and aim-point selection. The limiting factor is the crossrange resolution, which can be improved by flying an appropriate trajectory. Our analysis assumes a focused system, in which the radar returns from the scatterers are phase corrected for coherence.

The main factors impacting on the generation of appropriate trajectories have been discussed earlier. Note that imaging the target using DBS is not permissible for the whole of the terminal engagement, and some means of homing in on the target at short ranges is required. This issue is not addressed in this paper. The derivation of the DBS equations makes use of some basic radar formulas. The Doppler shift from a point on the ground is given as

$$f_D = 2(\boldsymbol{v}\cdot\boldsymbol{R})/\lambda \tag{A1}$$

where $\boldsymbol{R}$ is a unit vector aligned with the sightline axis and $\boldsymbol{v}$ is a vector aligned with a wind axes set. When the appropriate elements from the transformation matrices are used, the velocity vector and the unit sightline vector can be written in terms of space-orientated unit vectors $\boldsymbol{i}$, $\boldsymbol{j}$, and $\boldsymbol{k}$ as

$$\boldsymbol{v} = V[c(\gamma)c(\chi)\boldsymbol{i} + c(\gamma)s(\chi)\boldsymbol{j} + s(\gamma)\boldsymbol{k}] \tag{A2}$$

$$\boldsymbol{R} = c(\lambda_y)c(\lambda_z)\boldsymbol{i} + c(\lambda_y)s(\lambda_z)\boldsymbol{j} - s(\lambda_z)\boldsymbol{k} \tag{A3}$$

The vector dot product can be written as

$$\boldsymbol{v}\cdot\boldsymbol{R} = |\boldsymbol{v}||\boldsymbol{R}|\cos(\Omega) \tag{A4}$$

where Ω is the total angle between the velocity vector and the sightline vector. Hence,

$$\boldsymbol{v}\cdot\boldsymbol{R} = V\cos(\Omega) \tag{A5}$$

$$\Omega = c^{-1}[c(\lambda_z)c(\lambda_y)c(\gamma)c(\chi) + c(\gamma)s(\chi)c(\lambda_y)s(\lambda_z) - s(\gamma)s(\lambda_y)] \tag{A6}$$

$$f_D = 2V\cos(\Omega)/\lambda \tag{A7}$$

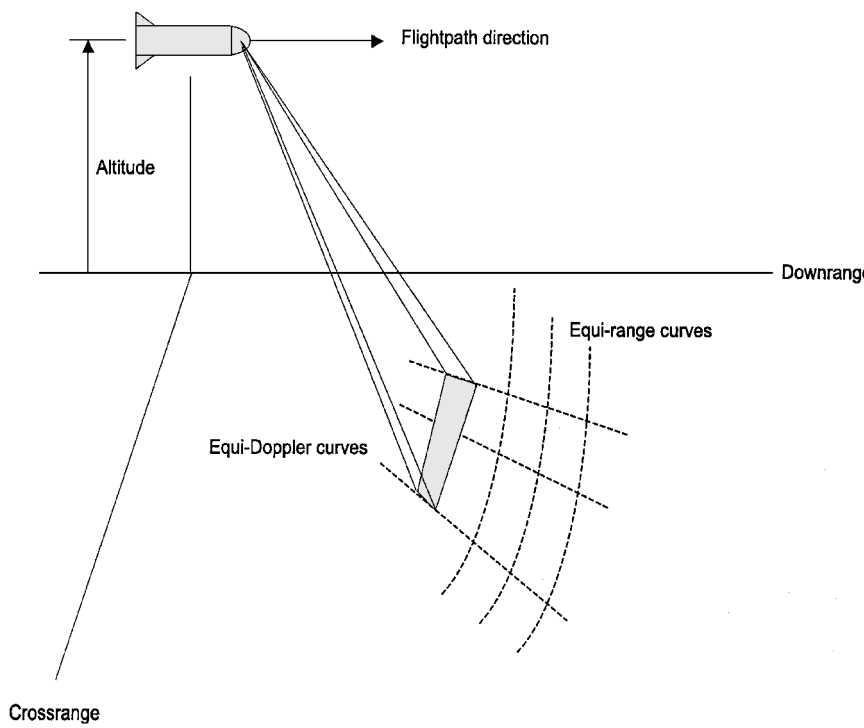

Fig. A1 DBS radar.

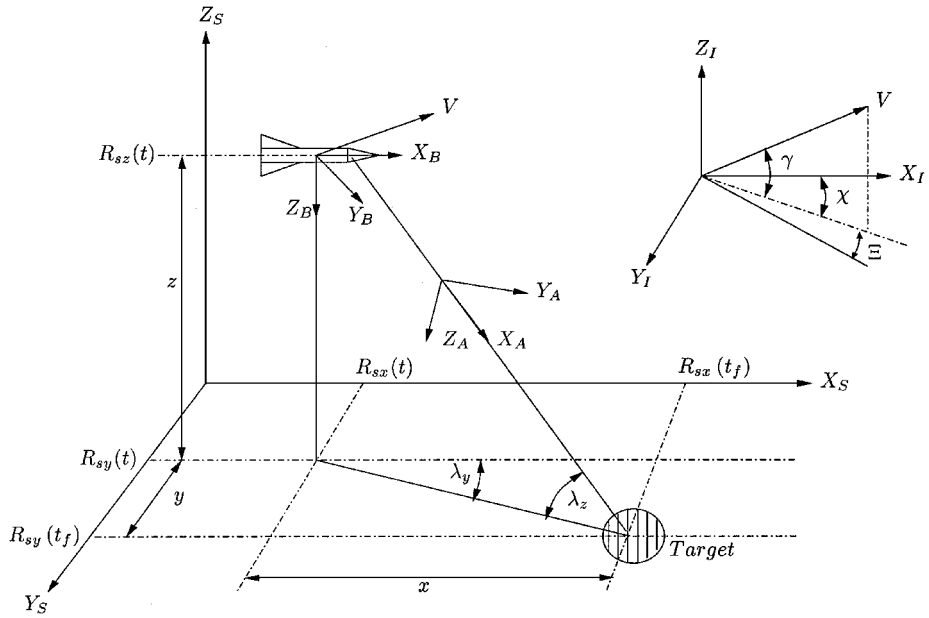

Fig. A2 DBS terminal guidance.

The total angle between the velocity vector and the sightline vector can be expressed as

$$\cos(\Omega) = \cos(\Xi)\cos(\Lambda) \tag{A8}$$

Now consider two points on the ground, A and B, for example, that need to be resolved in Doppler. Because the range to these points is different and the missile is traveling at velocity V, the Doppler shift at these points will be

$$f_{DA} = 2V\cos(\Xi)\cos(\Lambda)/\lambda \tag{A9}$$

$$f_{DB} = 2V\cos(\Xi + \delta\Xi)\cos(\Lambda)/\lambda \tag{A10}$$

Subtracting the Doppler difference gives

$$\Delta f_D = \{2V\cos(\Lambda)[\cos(\Xi) - \cos(\Xi)\cos(\delta\Xi) + \sin(\Xi)\sin(\delta\Xi)]\}/\lambda \tag{A11}$$

$$\Delta f_D \approx 2V\cos(\Lambda)\sin(\Xi)\delta\Xi/\lambda, \qquad \text{for small}\,\delta\Xi \tag{A12}$$

The Doppler resolution in crossrange is given by

$$1/\delta t = 2V[\cos(\Lambda)\sin(\Xi)\delta\Xi]/\lambda \tag{A13}$$

Rearranging yields

$$\delta\Xi = \lambda/2(V)(\delta t)\sin(\Xi)\cos(\Lambda) \tag{A14}$$

The crossrange resolution Δ is the product of the range R and the increment in azimuth angle between the velocity vector and sightline vector:

$$\Delta = R(\delta\Xi) = \frac{R\lambda}{2V(\delta t)\sin(\Xi)\cos(\Lambda)} \tag{A15}$$

In terms of the terminal guidance problem, it can be seen that the crossrange resolution is inversely proportional to the azimuth angle between the velocity vector and sightline, Ξ. Note that the angle Ξ will approach zero as the velocity and sightline vectors become aligned.

Now assume that the target has been acquired before the terminal guidance phase. This is shown in Fig. A2; it is assumed the target lies at ground level. Four frames of reference are shown in Fig. A2: 1) Earth-fixed frame (X_S, Y_S, Z_S), 2) missile body frame (X_B, Y_B, Z_B), 3) missile inertial frame (X_I, Y_I, Z_I), and 4) sightline frame (X_A, Y_A, Z_A).

It is assumed that the missile inertial frame and Earth-fixed frame are aligned with one another. We consider the engagement in the azimuth plane only to derive a simplified expression for the crossrange resolution. The simplified expression is used purely for optimization purposes; needless to say, in the figures where crossrange resolution is displayed, the correct expression (A15) is used. The simplified expression is exact for flight parallel to the x axis and zero elevation angle between the velocity vector and sightline, that is, an azimuth plane engagement with flight along the x axis. If we consider a planar engagement in the azimuth plane only, Eq. (A15) simplifies to

$$\Delta = \frac{\lambda\left(\sqrt{x^2 + y^2}\right)}{2V(\delta t)\sin(\Xi)} \tag{A16}$$

Now

$$\Xi = \lambda_y - \chi \tag{A17}$$

$$\sin(\lambda_y - \chi) = \sin(\lambda_y)\cos(\chi) - \cos(\lambda_y)\sin(\chi) \tag{A18}$$

From Fig. A2,

$$\sin(\lambda_y) = y\Big/\sqrt{x^2 + y^2} \tag{A19}$$

$$\cos(\lambda_y) = x\Big/\sqrt{x^2 + y^2} \tag{A20}$$

$$\cos(\chi) = V_{sx}/V\cos(\gamma) \tag{A21}$$

$$\sin(\chi) = V_{sy}/V\cos(\gamma) \tag{A22}$$

Substituting gives

$$\Delta = \frac{\lambda(x^2 + y^2)}{2(\delta t)[V_{sx}(y) - V_{sy}(x)]} \tag{A23}$$

For small χ, the following approximations are valid:

$$V \approx V_{sx}, \qquad V_{sy} \approx 0.0 \tag{A24}$$

Hence, the crossrange resolution simplifies to

$$\Delta = \frac{\lambda(x^2 + y^2)}{2V(\delta t)(y)} \tag{A25}$$

Acknowledgment

The results in this paper were supported by funding from Alenia Marconi Systems, Ltd.

References

[1]Kim, E., Cho, H., and Lee, Y., "Terminal Guidance of Missiles Maneuvering in the Vertical Plane," AIAA Guidance, Navigation, and Control Conf., July 1996.

[2]Kim, M., and Grider, K. V., "Terminal Guidance for Impact Attitude Constrained Flight Trajectories," *IEEE Transactions on Aerospace and Electronic Systems*, Vol. AES-9, No. 6, 1973, pp. 852–859.

[3]Green, M., and Limebeer, D. J. N., *Linear Robust Control*, Prentice–Hall International, Upper Saddle River, NJ, 1995.

[4]Song, T. L., and Shin, S. J., "Time Optimal Impact Angle Control for Vertical Plane Engagements," *IEEE Transactions on Aerospace and Electronic Systems*, Vol. 35, No. 2, 1999, pp. 738–742.

[5]Nasuti, F., and Innocenti, M., "Missile Trajectory Optimization with Agility Issues," AIAA Paper 96-3730, July 1996.

[6]Kumar, R., Seywald, H., Cliff, E., and Kelley, H. J. M., "Three Dimensional Air-to-Air Missile Trajectory Shaping," *Journal of Guidance, Control, and Dynamics*, Vol. 18, No. 3, 1995, pp. 449–456.

[7]Kumar, R., Seywald, H., and Cliff, E., "Near Optimal Three-Dimensional Guidance Against Maneuvering Target," *Journal of Guidance, Control, and Dynamics*, Vol. 18, No. 3, 1995, pp. 457–464.

[8]Lu, P., and Pierson, B. L., "Optimal Aircraft Terrain-Following Analysis and Trajectory Generation," *Journal of Guidance, Control, and Dynamics*, Vol. 18, No. 3, 1995, pp. 555–560.

[9]Menon, P. K. A., Kim, E., and Cheng, V. H. L., "Optimal Trajectory Synthesis for Terrain-Following Flight," *Journal of Guidance, Control, and Dynamics*, Vol. 14, No. 4, 1991, pp. 807–813.

[10]Lu, P., and Pierson, B. L., "Aircraft Terrain-Following Based on a Nonlinear Continuous Predictive Control Approach," *Journal of Guidance, Control, and Dynamics*, Vol. 18, No. 1, 1995, pp. 817–823.

[11]Grimm, W., and Hiltmann, P., "Direct and Indirect Approach for Real-Time Optimization of Flight Paths," *Proceedings of the Conference on Optimal Control and Variational Calculus*, edited by R. Bulirsch, A. Miele, J. Stoer, and K. H. Well, Lecture Notes in Control and Information Sciences, Springer-Verlag, 1987.

[12]Betts, J. T., "Sparse Jacobian Updates in the Collocation Method for Optimal Control Problems," *Journal of Guidance, Control, and Dynamics*, Vol. 13, No. 3, 1990, pp. 409–415.

[13]Skalecki, L., and Martin, M., "Application of Multiple Shooting to Closed Loop Guidance," International Astronautical Federation, IAF Paper 91-326, Oct. 1991.

[14]Skalecki, L., and Martin, M., "General Adaptive Guidance Using Nonlinear Programming Constraint-Solving Methods," *Journal of Guidance, Control, and Dynamics*, Vol. 16, No. 3, 1993, pp. 517–522.

[15]Kumar, R., and Seywald, H., "Dense-Sparse Discretization for Optimization and Real-Time Guidance," *Journal of Guidance, Control, and Dynamics*, Vol. 19, No. 2, pp. 501–503.

[16]Pytlak, R., and Vinter, R. B., "A Feasible Directions Type Algorithm for Optimal Control Problems With Hard State and Control Constraints," *IEEE Proceedings of the 32nd Conference on Decision and Control*, Inst. of Electrical and Electronics Engineers, New York, 1993, pp. 3335–3340.

[17]Pytlak, R., and Vinter, R. B., "A Feasible Directions Algorithm for Optimal Control Problems with State and Control Constraints: Implementation," *Journal of Optimization Theory and Applications*, Vol. 191, 1999, pp. 623–649.

[18]Pytlak, R., and Vinter, R. B., "Second Order Method for Optimal Control Problems with Hard State and Control Constraints," *IEEE Proceedings of the 34th Conference on Decision and Control*, Inst. of Electrical and Electronics Engineers, New York, 1995, pp. 625–630.

[19]Pytlak, R., *Numerical Methods for Optimal Control Problems with State Constraints*, Lecture Notes in Mathematics, Springer-Verlag, Berlin, 1999.

[20]Garnell, P., and East, D., *Guided Weapon Control Systems*, Pergamon, Oxford, 1980.

[21]Minzner, R. A., Champion, K. S. W., and Pond, H. L., "The ARDC Model Atmosphere," U.S. Air Force Cambridge Research Center, Bedford, MA, 1959.

[22]Hovanessian, S. A., *Radar Detection and Tracking Systems*, Artech House, Dedham, MA, 1983, Chap. 7.

[23]Edde, B., *Radar: Principles, Technology and Applications*, Prentice–Hall, Upper Saddle River, NJ, 1993, pp. 616–652.

[24]Franceschetti, G., and Lanari, R., *Synthetic Aperture Radar Processing*, CRC Press, Boca Raton, FL, 1999.